Transition Metal Chemistry (2019) 44:107–114
https://doi.org/10.1007/s11243-018-0274-9

# Structures and photocatalytic performance of two $d^{10}$ metal-based coordination polymers containing mixed building units

Lu Lu[1] · Jun Wang[1] · Feng Chen[1] · Lin-Tao Wei[2] · Li-Min Lin[2] · Bao-Hong Li[2] · Amita Singh[3] · Abhinav Kumar[3]

Received: 2 August 2018 / Accepted: 5 September 2018 / Published online: 3 October 2018


## Abstract

The linker 1,4-bis(2-methyl-imidazole-yl)-butane (bib) was used to construct two coordination polymers, specifically $[Cd(bib)(ipa)]_n$ (**1**) and $[Zn(bib)(tpa)]_n$ (**2**), in the presence of isophthalic acid ($H_2$ipa) and terephthalic acid ($H_2$tpa), respectively, under solvothermal conditions. Topological analyses reveal that the crystal of complex **1** consists of a 3D threefold interpenetrating network with Schläfli symbol $\{6^5.8\}$, while complex **2** possesses a 2D wavelike layer structure with Schläfli symbol $\{6^6\}$. The photocatalytic properties of both complexes for the degradation of methyl violet have been explored, revealing that complex **2** is a better photocatalyst than **1**. A mechanism for the photocatalytic properties of the complexes is proposed, based on the results of density of states (DOS) and partial DOS calculations.

## Introduction

The photodegradation of organic dyes based on azo groups (–N=N–) as chromophore is an important objective. However, conventional semiconductor photocatalyst does not give optimal results in this application [1, 2]. Coordination polymers (CPs), as a new kind of photocatalytic materials with attractive physical properties and versatile architectures, have attracted significant attention in the purification of water by sustainable decomposition of organic dyes [1–9]. In CPs used as photocatalysts, the different types of interactions between their inorganic and organic moieties may lead to diverse metal–organic ligand charge transfer interactions [10]. Some important CPs [such as UIO-66, ZIF-8 and MIL-100(Fe)] have been found to possess excellent photocatalytic properties [11–14]. Therefore, the controlled construction of novel CPs offers much potential for the development of photocatalysts for the degradation of organic dyes in the presence of light. An essential consideration in the construction of CP-based photocatalysts is the selection of appropriate organic ligands [15, 16].

In continuation to our efforts to develop new CPs with photocatalytic properties [17–19], in this work, the linker 1,4-bis(2-methyl-imidazole-yl)-butane (bib) (Scheme 1) was used to construct CPs in the presence of two aromatic dicarboxylate co-linkers displaying configurational isomerism, namely isophthalic acid ($H_2$ipa) and terephthalic acid ($H_2$tpa) (Scheme 1). Two CPs, namely $[Cd(bib)(ipa)]_n$ (**1**) and $[Zn(bib)(tpa)]_n$ (**2**), were synthesized and characterized, and their photocatalytic properties for the photodecomposition of methyl violet (MV) as a representative organic dye have been investigated. The results of these investigations are presented herein.

**Electronic supplementary material** The online version of this article (https://doi.org/10.1007/s11243-018-0274-9) contains supplementary material, which is available to authorized users.

✉ Lu Lu
lulusczg@126.com

✉ Bao-Hong Li
gdmcli@126.com

✉ Abhinav Kumar
abhinavmarshal@gmail.com

[1] School of Chemistry and Environmental Engineering, Sichuan University of Science and Engineering, Zigong, People's Republic of China

[2] Dongguan Key Laboratory of Drug Design and Formulation Technology, Key Laboratory of Research and Development of New Medical Materials of Guangdong Medical University, School of Pharmacy, Guangdong Medical University, Dongguan 523808, People's Republic of China

[3] Department of Chemistry, Faculty of Science, University of Lucknow, Lucknow 226 007, India

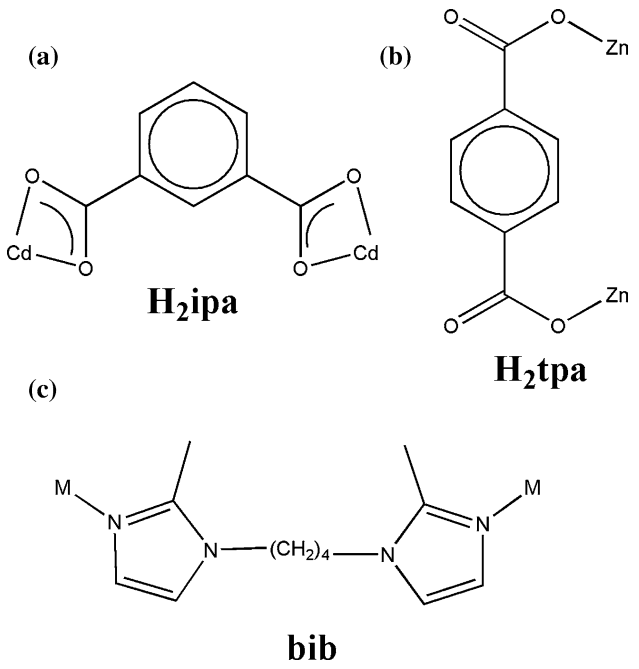


**Scheme 1** **a**–**c** The different coordination modes of the ligands used in this work

## Experimental

### Materials and methods

All the chemicals were procured from commercial sources and used without further purification. The powder X-ray diffraction (PXRD) data were collected on a Bruker D8 ADVANCE X-ray diffractometer equipped with Cu-Kα radiation ($\lambda = 1.5418$ Å) at 50 kV, 20 mA with a scanning rate of 6°/min and a step size of 0.02°. The simulated powder patterns for both complexes were obtained using Mercury 2.0 software. FTIR spectra as KBr pellets were recorded using a Nicolet Impact 750 FTIR spectrometer in the range of 400–4000 $cm^{-1}$. Thermogravimetric analysis (TGA) was performed under a nitrogen atmosphere from room temperature to 650 °C at a heating rate of 10 °C $min^{-1}$, using a SDT Q600 thermogravimetric analyzer.

### Crystal structure determination

The single-crystal X-ray diffraction data were obtained on a Bruker SMART APEX diffractometer equipped with graphite monochromated Mo-Kα radiation ($\lambda = 0.71073$ Å) by using the $\omega$-scan technique at 100 K. The intensities were corrected for absorption effects using SADABS. The structures were solved by direct methods (SHLEXS-2014) and refined using full-matrix least-squares procedures based on $F^2$ (SHELXL-2014) [20]. All the hydrogen atoms were generated geometrically and refined isotropically using a riding model. All the non-hydrogen atoms were refined with anisotropic displacement parameters. The disordered atoms of the propyl chain in complex **1** were not included in the models. The disordered atoms of complex **1** (C13, C14, C15, C16) were refined using C atoms split over two sites, with a total occupancy of 1. It was found the Flack parameter for the structure was 0.16(4), and hence the twin refinement was used to get the final structure. The crystallographic details and selected bond dimensions for both complexes are listed in Tables 1 and 2. CCDC numbers are 1839730 for **1** and 1839735 for **2**.

### Synthesis of $[Cd(bib)(ipa)]_n$ (1)

A mixture of $H_2$ipa (0.10 mmol, 0.017 g), bib (0.10 mmol, 0.022 g), $Cd(NO_3)_2{\cdot}4H_2O$ (0.15 mmol, 0.027 g) and 20 mL of DMF/$H_2O$ ($v/v = 3{:}1$) was stirred for 30 min and then transferred and sealed into a 25-mL Teflon-lined reactor. The mixture was heated to 120 °C for 72 h and then cooled to room temperature at a rate of 5 °C/h. Yellow block crystals of complex **1** were obtained in 46% yield based on bib. IR data (KBr, $cm^{-1}$) are 3100 (m), 2943 (m), 2341 (m), 1603 (vs), 1539 (m), 1490 (m), 1375 (vs), 1269 (v), 994 (m), 737 (m).

### Synthesis of $[Zn(bib)(tpa)]_n$ (2)

A mixture of $H_2$tpa (0.10 mmol, 0.017 g), bib (0.10 mmol, 0.022 g), $Zn(NO_3)_2{\cdot}6H_2O$ (0.15 mmol, 0.047 g) and 10 mL of DMF/$H_2O$ ($v/v = 1{:}1$) was stirred for 30 min and then transferred and sealed into a 25-mL Teflon-lined reactor. The mixture was heated to 120 °C for 72 h and then cooled to room temperature at a rate of 5 °C/h. Colorless block crystals of complex **2** were obtained in 57% yield based on bib. IR data (KBr, $cm^{-1}$) are 3090 (m), 2341(m), 1615 (vs), 1501 (m), 1408 (m), 1346 (v), 1276 (m), 1147 (m), 1001 (m), 825 (v), 731 (vs), 573 (m).

### Photocatalytic reactions

The photocatalytic reactions were performed as follows. A sample of complex **1** or **2** (50 mg) was dispersed in 50 mL of an aqueous solution of MV (10 mg/L) under stirring in the dark for 30 min to ensure the establishment of an adsorption–desorption equilibrium. The mixture was then exposed to UV irradiation using an Hg lamp (250 W) and kept under continuous stirring during irradiation for 100 min. Aliquots of 5 mL volume were taken out after every 10 min and separated by centrifugation for analyses by UV–Vis

spectrometer. A control experiment was also performed under the same conditions but without adding the catalysts.

### Computational details

The probable mechanism for the photodegradation of organic dyes in the presence of CPs as photocatalysts has been addressed by band gap calculations. The smallest unit of both CPs was geometry-optimized using the B3LYP functional [21, 22], and the 6-31G** basis set for all the atoms except the metal centers, for which the CEP-121G basis set was employed. All the calculations were carried out with the Gaussian 09 program [23]. GaussSum 3.1 was used to obtain density of state (DOS) plots [24].

## Results and discussion

### Structure description of complex 1

Each asymmetric unit of complex **1** comprises one independent Cd(II) center, one bib ligand and one fully deprotonated ipa ligand. The Cd(II) center has an octahedral $\{CdO_4N_2\}$ geometry, being coordinated by four carboxylate oxygen atoms and two imidazole nitrogen atoms (Fig. 1a). The $ipa^{2-}$ ligand adopts a bidentate chelating coordination mode ($\mu_2-\eta^1:\eta^1$) that bridges Cd(II) centers to produce chains of $[Cd(ipa)]_n$ units along the *b*-axis with a pitch of 17.12 Å. The bib ligand adopts a *syn-anti* coordination geometry to bridge the Cd(II) centers into a 1D chain of $[Cd(bib)]_n$ units. The $[Cd(ipa)]_n$ chains are further connected by the $[Cd(bib)]_n$ chains to form a 3D structure (Fig. 1b). To understand the structure more clearly, topological analysis has been used to simplify the framework. If the ipa and bib ligands are considered as connecters, the Cd(II) centers can be viewed as four-connected nodes; hence, the whole topology of the 3D structure can be simplified as a uninodal four-connected net with the Schläfli symbol $\{6^5.8\}$, calculated using TOPOS software (Fig. 1c). The potential voids are large enough to allow three independent identical networks, leading to a 3D threefold interpenetrating architecture (Fig. 1d). CP **1** is iso-reticular with [Co(bib)(aipa)] and [Co(bib)(glu)] ($H_2$aipa = 5-aminoisophthalic acid and $H_2$glu = glutaric acid) [25], which show single-crystal-to-single-crystal (SCSC) transformations.

### Structure description of complex 2

CP **2** crystallizes in the monoclinic space group $P_2/c$ and can be described as a 2D network. The asymmetric unit includes

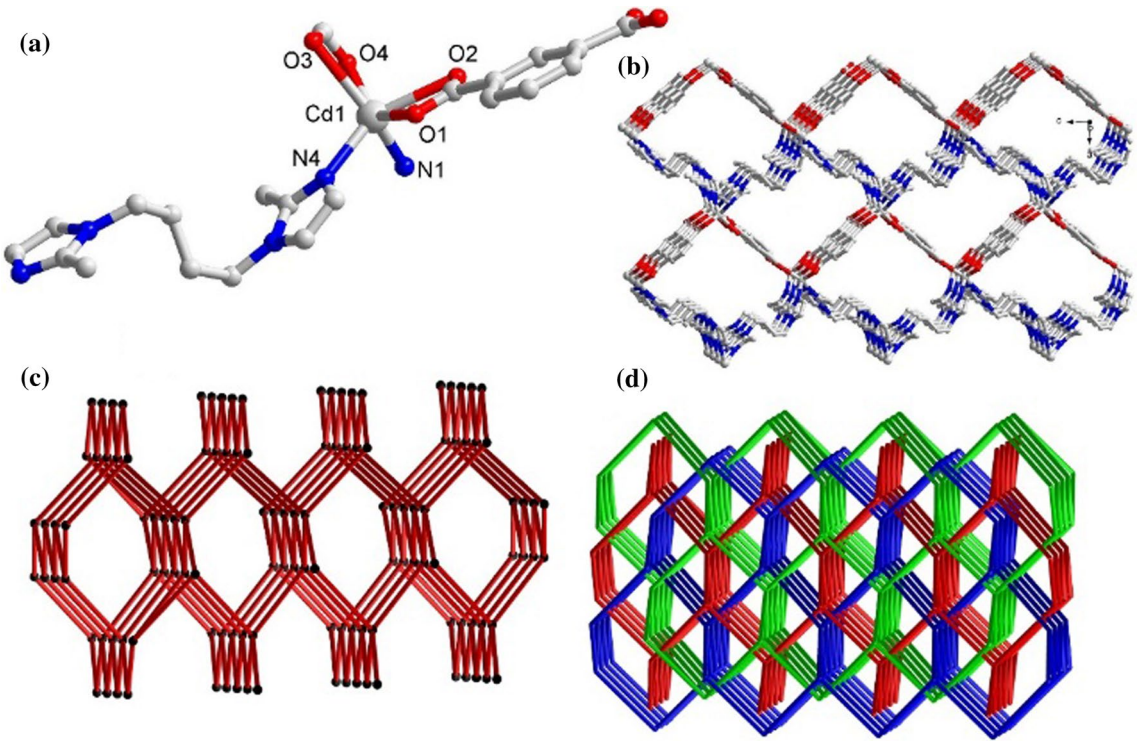


**Fig. 1** **a** Perspective view of the coordination geometry around the metal center in complex **1**; **b** the 3D microporous metal–organic framework; **c** schematic diagram four-connected topology; **d** view of threefold interpenetrating net

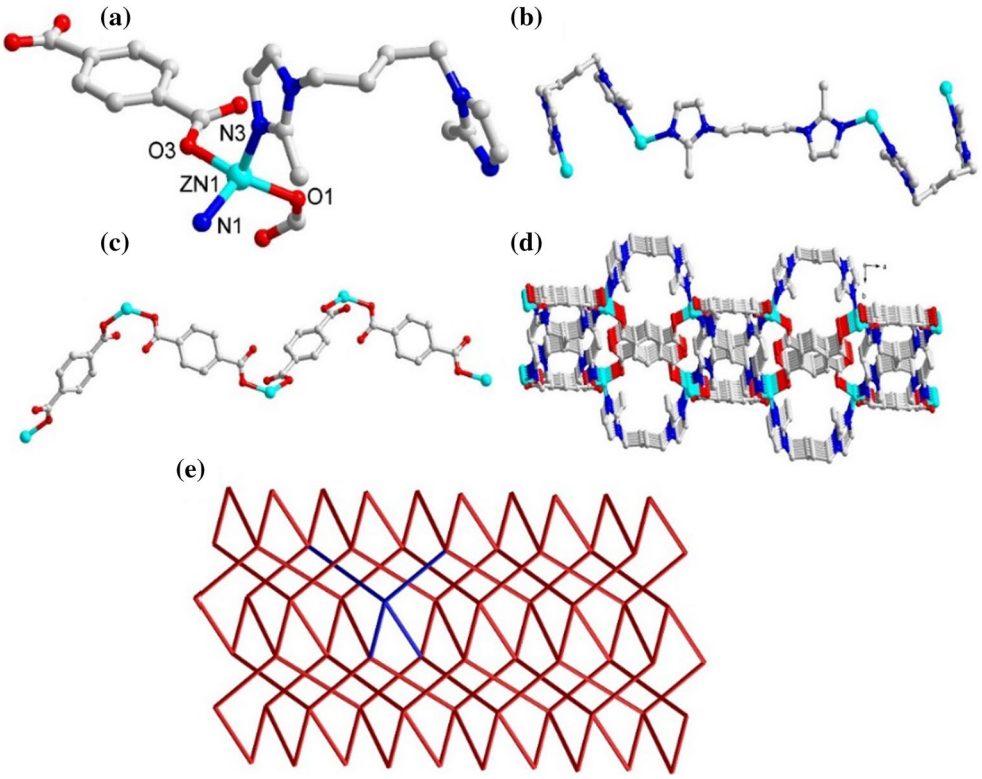


**Fig. 2** **a** Perspective view of the coordination mode around the Zn(II) center in complex **2**; **b** the 1D chain formed by Zn(II) and bib; **c** the 1D chain formed by Zn(II) and tpa ligands; **d** 2D layer; **e** the schematic topological network

one Zn(II) center, one bib ligand and one tpa ligand. Each Zn(II) center is four-coordinated by two carboxylate oxygen atoms (O1 and O3) and two imidazole nitrogen atoms (N1 and N3) (Fig. 2a). The Zn–O and Zn–N distances are 1.949(4), 1.997(6), 2.025(4) and 2.033(4) Å, respectively (Table S1). The Zn(II) centers are bridged by the carboxylic groups of the $tpa^{2-}$ anions to form a 1D zig-zag chain (Fig. 2b). The bib ligand also adopts *syn-anti* coordination to connect the Zn(II) centers, giving a 1D zig-zag chain (Fig. 2c). These $[Zn(bib)]_n$ chains are further connected by the 1D zig-zag $[Zn(tpa)]_n$ chains to generate a 2D wave-like network (Fig. 2d), which can be simplified as a four-connected network with the Schläfli symbol $\{6^6\}$(Fig. 2e).

## IR, powder X-ray diffraction (PXRD) and thermal analyses

The IR spectra of both CPs display characteristic bands in the range of 1400–1610 $cm^{-1}$ which can be attributed to the asymmetric and symmetric stretching vibrations of the carboxylato groups. The values of $\Delta\nu[\nu_{as}(COO)-\nu_{s}(COO)]$ are 113 and 207 $cm^{-1}$ for **1** and **2**, respectively, indicating bidentate and monodentate coordination modes of the carboxylato groups, respectively (Fig. S1) [26]. A band at ca. 1500 $cm^{-1}$ for complex **1** can be assigned to $\nu$(C=N) absorption of the imidazole rings of the bib ligand. To determine whether the crystal structures are truly representative of the bulk materials used for property studies, X-ray powder diffraction (PXRD) experiments were carried out for both CPs (Fig. 3). The diffraction peaks of the experimental and simulated patterns are a good match, indicating the phase purity of the bulk samples.

To assess their thermal stabilities, thermogravimetric analyses (TGA) for both CPs were performed under a nitrogen atmosphere (Fig. S2). The frameworks of both were thermally stable up to ~ 350 °C, after which decomposition of both CPs commenced.

## Photocatalysis

The photocatalytic performances of both complexes for the degradation of methyl violet as a model organic dye were investigated. The photodegradation experiments were carried out under UV irradiation after achieving adsorption equilibrium in the dark. The photocatalytic results for both CPs are presented in Fig. 4. In both cases, the UV–Vis band corresponding to MV decreases progressively with reaction time (Fig. 4a, b). The UV–Vis band intensities of MV at 506 nm against reaction time ($t$) were plotted for both CPs (Fig. 4c). The results indicate that approximately 46% of MV in the presence of **1** and 71% of MV in the presence of

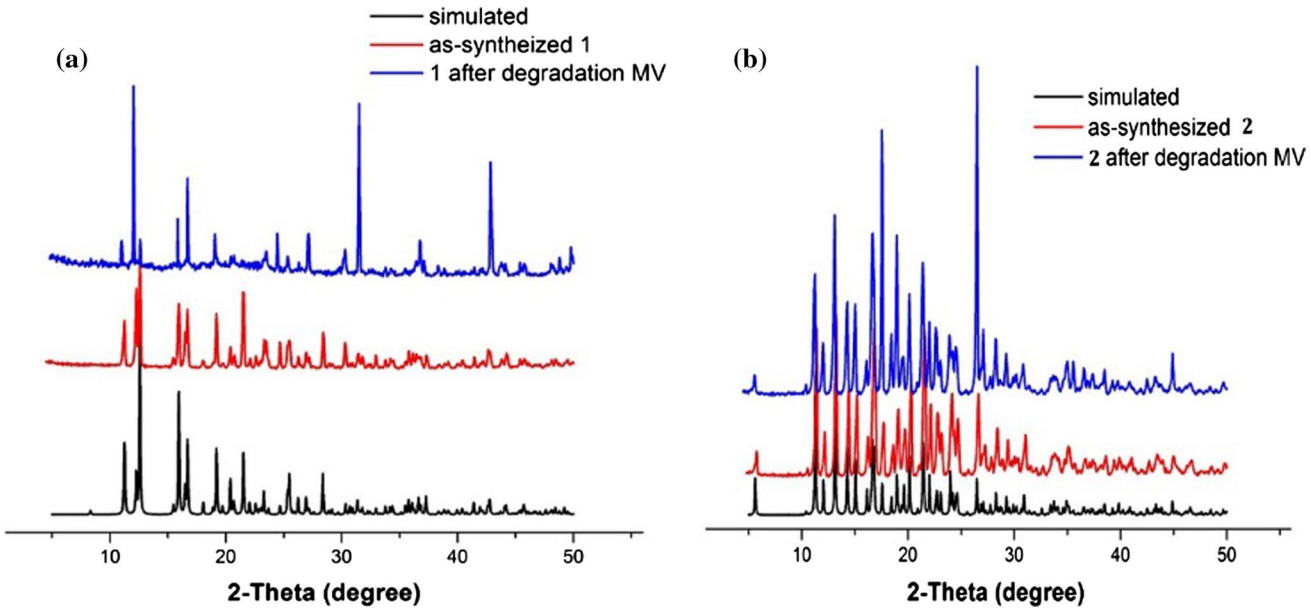


**Fig. 3** **a** Simulated and experimental PXRD patterns of complex **1**. **b** Simulated and experimental PXRD patterns of complex **2**

**2** were decomposed after 40 min. In addition, control experiments on the photodegradation of MV carried out under similar reaction conditions showed decomposition of MV only up to 23%. Overall, the photocatalytic results indicate that catalyst **2** is more active for the decomposition of MV than **1** [27, 28].

The structural integrity of both CPs after photodegradation of MV was assessed with the help of PXRD experiments. The PXRD results indicate that the crystallinity of both CPs was well maintained, even after degradation of MV (Fig. 3). The different catalytic activities of the two CPs can be attributed to the use of isomeric co-ligands, coordination modes of the metal centers and the differences of the final frameworks [29, 30].

To gain a better understanding of the mechanism of photocatalysis of MV by both these CPs, the band structures of both **1** and **2** have been calculated using density functional theory. As presented in Fig. 5, the valence band lying just below the Fermi levels of both complexes is mainly contributed by the aromatic centers as well as the oxygen and nitrogen atoms with negligible contributions from the Cd center in **1** and Zn center in **2**. Also, the conduction band for CP **1** which lies just above the Fermi level in the range of −1.31 to −0.59 eV is derived from the aromatic moieties with admixture of the oxygen atoms. Similarly, in the case of CP **2**, the conduction band above the Fermi level lying in the range of −1.38 to −0.77 eV has contributions from the aromatic carbons and oxygen atoms. Hence, as evident from the pDOS plots, the electronic transitions in both CPs are mainly operating from the aromatic center to another aromatic region (ligand-to-ligand) with no contribution from the metal centers. Hence, in the typical photocatalytic process, CPs **1** and **2** undergo excitation by light to generate electron–hole pairs. The holes then migrate to the metal center, while the electron migrates to the ligand.

It is apparent that CP **2** displays better catalytic efficiency toward the degradation of MV. This may be due to the better ability of the Zn(II) centers to facilitate formation of the hydroxyl radical (OH·) on the coordination network, although this feature requires further investigation [31, 32]. Although catalysts **1** and **2** possess similar ligands, their different metals may result in distinct band gap sizes, explaining the differences in their photocatalytic activities [33, 34].

## Conclusion

In summary, the linker 1,4-bis(2-methyl-imidazole-yl)-butane (bib) has been utilized to construct two new coordination polymers from isomeric aromatic dicarboxylic acid ligands. We obtained two different frameworks: a 3D threefold interpenetrating network with Schläfli symbol $\{6^5.8\}$ in the case of **1**, and a 2D wavelike layer structure with Schläfli symbol $\{6^6\}$ for **2**. Both CPs show photocatalytic properties for the photodegradation of MV dye. Hence, these results provide information for the further development of designed frameworks that can provide efficient catalytic systems for the photodegradation of aromatic dyes.

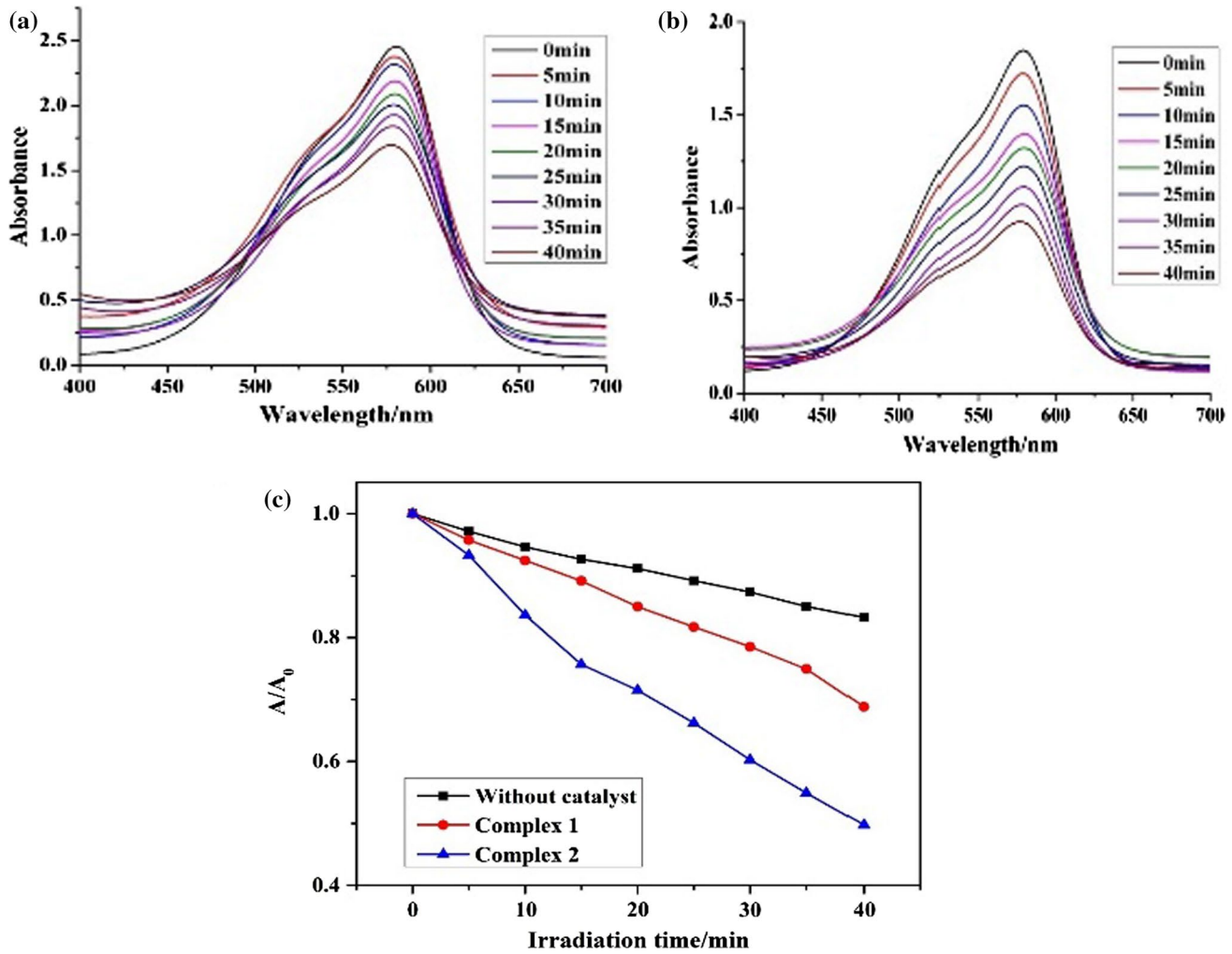


**Fig. 4** **a**, **b** UV–Vis absorption spectra of MV solutions during decomposition by complex **1** and **2**, respectively; **c** photocatalytic degradation of MV under UV with the use of complex **1** and **2**; the black curve is the control experiment without any catalyst

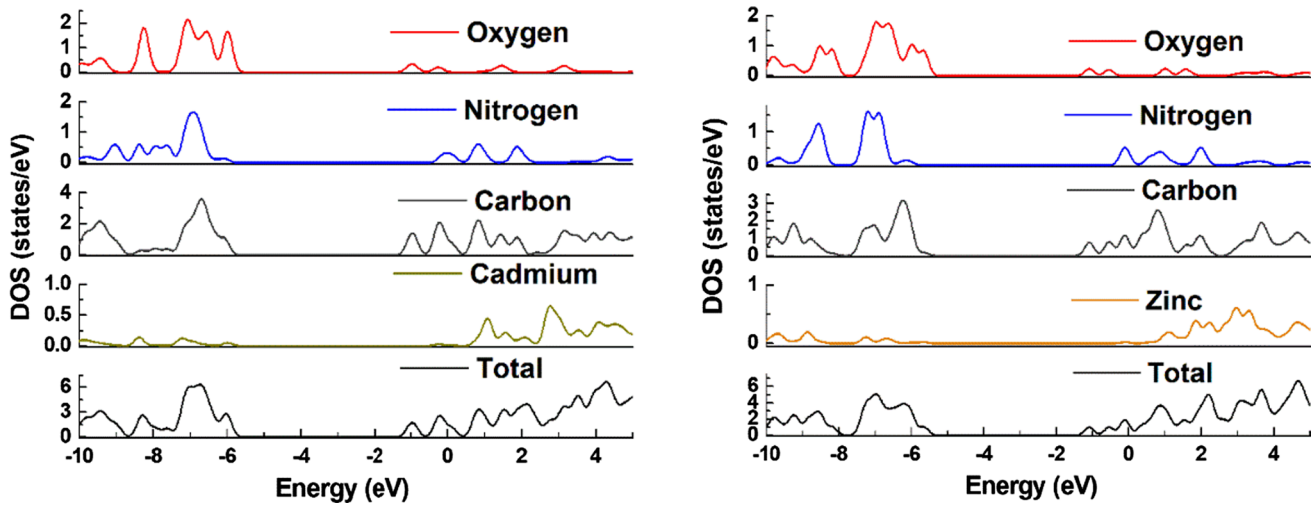


**Fig. 5** Density of states (DOS) and partial DOS plots for **1** (left) and **2** (right)

**Table 1** Crystallographic data and structures refinement details for **1** and **2**

| Parameter | **1** | **2** |
|---|---|---|
| Formula weight | 494.81 | 447.78 |
| Crystal system | Orthorhombic | Monoclinic |
| Space group | $Pna2_1$ | $P2/c$ |
| Crystal color | Yellow | Colorless |
| $a$ (Å) | 9.3921 (6) | 15.9224 (19) |
| $b$ (Å) | 14.4190 (8) | 10.0901 (12) |
| $c$ (Å) | 15.6612 (9) | 12.6885 (16) |
| $\alpha$ (°) | 90 | 90 |
| $\beta$ (°) | 90 | 99.955 (3) |
| $\gamma$ (°) | 90 | 90 |
| $V$ (Å$^3$) | 2120.9 (2) | 2007.8 (4) |
| $Z$ | 4 | 4 |
| $\rho_{calcd}$ (g/cm$^3$) | 1.550 | 1.481 |
| $\mu$ (mm$^{-1}$) | 1.062 | 1.258 |
| $F$(000) | 1000 | 928 |
| $\theta$ Range (°) | 2.6–27.6 | 2.0–27.6 |
| Reflection collected | 12,223 | 11,867 |
| Independent reflections ($R_{int}$) | 0.020 | 0.062 |
| Reflections with $I > 2\sigma(I)$ | 4150 | 4597 |
| Number of parameters | 272 | 264 |
| $R_1$, $wR_2(I > 2\sigma(I))$[a] | 0.0277, 0.0785 | 0.0618, 0.1560 |
| $R_1$, $wR_2$ (all data)[b] | 0.0312, 0.0816 | 0.1207, 0.1849 |

[a] $R = \sum(F_o - F_c)/\sum(F_o)$

[b] $wR_2 = \{\sum[w(F_o^2 - F_c^2)^2]/\sum(F_o^2)^2\}^{1/2}$

**Table 2** Selected bond distances (Å) and angles (°) for **1** and **2**

| | | | |
|---|---|---|---|
| **1** | | | |
| Cd(1)–O(1) | 2.255 (4) | Cd(1)–O(2) | 2.501 (6) |
| Cd(1)–N(1) | 2.279 (5) | Cd(1)–O(3)#1 | 2.592 (6) |
| Cd(1)–O(4)#1 | 2.213 (5) | Cd(1)–N(4)#2 | 2.257 (4) |
| **2** | | | |
| Zn(1)–O(1) | 1.949 (5) | Zn(1)–O(3) | 1.998 (6) |
| Zn(1)–N(1) | 2.025 (5) | Zn(1)–N(3) | 2.033 (4) |
| **1** | | | |
| O(1)–Cd(1)–O(2) | 53.44 (17) | O(1)–Cd(1)–N(1) | 117.38 (17) |
| O(1)–Cd(1)–O(3)#1 | 98.99 (17) | O(1)–Cd(1)–O(4)#1 | 137.94 (16) |
| O(2)–Cd(1)–N(1) | 91.85 (18) | O(2)–Cd(1)–O(3)#1 | 101.66 (19) |
| O(2)–Cd(1)–O(4)#1 | 96.99 (18) | O(2)–Cd(1)–N(4)#2 | 138.92 (18) |
| O(3)#1–Cd(1)–N(1) | 141.85 (17) | O(4)#1–Cd(1)–N(1) | 89.30 (16) |
| N(1)–Cd(1)–N(4)#2 | 93.12 (16) | | |
| **2** | | | |
| O(1)–Zn(1)–O(3) | 129.0 (2) | O(1)–Zn(1)–N(1) | 117.66 (17) |
| O(1)–Zn(1)–N(3) | 100.39 (18) | O(3)–Zn(1)–N(1) | 98.2 (2) |
| O(3)–Zn(1)–N(3) | 104.57 (19) | N(1)–Zn(1)–N(3) | 104.40 (17) |

Symmetry Codes for **1**: #1 = 1 − $x$, 2 − $y$, 1/2 + $z$; #2 = 5/2 − $x$, 1/2 + $y$, 1/2 + $z$

**Acknowledgements** The authors acknowledge financial assistance from Sichuan University of Science and Engineering (Nos. 2015RC26, 2015RC29 and 2017RCL02), the Education Committee of Sichuan Province (Nos. 17ZA0264, 17ZB0312, 18ZB0422, 18ZB0425), the Project of Zigong Science and Technology (No. 2016HG06), the Opening Project of Key Laboratory of Green Catalysis of Sichuan Institutes of High Education (No. LYJ1705) and Innovative Entrepreneurial Training Plan of undergraduates in Guangdong Province (Nos. 201810571008, 201810571012, 201810571047, 201810571082, 201810571061, 201810571091).

## References

1. Yoon MY, Srirambalaji R, Kim K (2012) Chem Rev 112:1196
2. Chen CC, Ma WH, Zhao JC (2010) Chem Soc Rev 39:4206
3. Wen T, Zhang DX, Zhang J (2013) Inorg Chem 52:12
4. Wang XL, Han N, Lin HY, Tian AX, Liu GC, Zhang JW (2014) Dalton Trans 43:2052
5. Zhang LN, Lu ST, Zhang C, Du CX, Hou HW (2015) CrystEngComm 17:846
6. Wang FQ, Wang CM, Yu JC, Xu KH, Li XY, Fu YY (2016) Polyhedron 105:49
7. Mu B, Li CX, Song M, Ren YL, Huang RD (2016) CrystEngComm 18:3086
8. Liao ZL, Li GD, Bi MH, Chen JS (2008) Inorg Chem 47:11
9. Guo J, Yang J, Liu YY, Ma JF (2012) CrystEngComm 14:6609
10. Li HX, Zhang XY, Huo YN, Zhu J (2007) Environ Sci Technol 41:4410
11. Wang SB, Wang XC (2015) Small 11:3097
12. Gao YW, Li SM, Li YX, Yao LY, Zhang H (2017) Appl Catal B Environ 202:165
13. Silva CG, Corma A, García A (2010) J Mater Chem 20:3141
14. So MC, Wiederrecht GP, Mondloch JE, Huppand JT, Farha OK (2015) Chem Commun 51:3501
15. Liu J, Wu J, Li F, Liu W, Li B, Wang J, Li Q, Yadav R, Kumar A (2016) RSC Adv 6:31161
16. Jin JC, Wu XR, Luo ZD, Deng FY, Liu JQ, Singh A, Kumar A (2017) CrystEngComm 19:4368
17. Wang J, Wu X, Liu J, Li B, Singh A, Kumar A, Batten SR (2017) CrystEngComm 19:3519
18. Lu L, Wang J, Xie B, Liu J, Yadav R, Singh A, Kumar A (2017) New J Chem 41:3537
19. Wang J, Bai C, Hu HM, Yuan F, Xue GL (2017) J Solid State Chem 249:87
20. Sheldrick GM (2015) Acta Crystallogr Sect A Found Adv 71:3
21. Becke AD (1993) J Chem Phys 98:5648
22. Lee CT, Yang WT, Parr RG (1998) Phys Rev B Condens Matter Mater Phys 37:785
23. Frisch MJ, Trucks GW, Schlegel HB, Scuseria GE, Robb MA, Cheeseman JR, Montgomery JA, Vreven JT, Kudin KN, Burant JC, Millam JM, Iyengar SS, Tomasi, J, Barone V, Mennucci B, Cossi M, Scalmani G, Rega N, Petersson GA, Nakatsuji H, Hada M, Ehara M, Toyota K, Fukuda R, Hasegawa J, Ishida M, Nakajima T, Honda Y, Kitao O, Nakai H, Klene M, Li X, Knox JE, Hratchian HP, Cross JB, Bakken V, Adamo C, Jaramillo J, Gomperts R, Stratmann RE, Yazyev O, Austin AJ, Cammi R, Pomelli C, Ochterski J W, Ayala PY, Morokuma K, Voth GA, Salvador P, Dannenberg JJ, Zakrzewski VG, Dapprich S, Daniels AD, Strain MC, Farkas O, Malick DK, Rabuck AD, Raghavachari K, Foresman JB, Ortiz JV, Cui Q, Baboul AG, Clifford S, Cioslowski J, Stefanov BB, Liu G, Liashenko A, Piskorz P, Komaromi I, Martin RL,Fox DJ, Keith T, Al-Laham MA, Peng CY, Nanayakkara A, Challacombe M, Gill PMW, Johnson B, Chen W, Wong WM,

Gonzalez C, Pople JA (2009) Gaussian 09 revision B.01, Gaussian, Inc., WallingFord CT
24. O'Boyle NM, Tenderholt AL, Langner KM (2008) J Comput Chem 29:839
25. Zhou HF, He T, Yue KF, Liu YL, Zhou CS, Yan N, Wang Y (2016) Cryst Growth Des 16:3961
26. Hu JM, Guo R, Liu YG, Cui GH (2016) Inorg Chim Acta 450:418
27. Mitkina TV, Zakharchuk NF, Naumov DY, Gerasko OA, Fenske D, Fedin VP (2008) Inorg Chem 47:6748
28. Britten J, Hearns NGR, Preuss KE, Richardson JF, Bin-Salamon S (2007) Inorg Chem 46:3934
29. Meng JX, Lu Y, Li YG, Fu H, Wang EB (2011) CrystEngComm 13:2479
30. Guo J, Yang J, Liu YY, Ma JF (2012) CrystEngComm 14:6609
31. Mahata P, Madras G, Natarajan S (2006) J Phys Chem B 110:13759
32. Gong Y, Li J, Qin J, Wu T, Cao R, Li J (2011) Cryst Growth Des 11:1662
33. Wang CM, Wang FQ, Dong CF, Yu ZC, Wang ZC, Zhao YN, Li GD (2015) Z Anorg Allg Chem 641:1125
34. Wang FQ, Dong CF, Wang ZC, Cui YR, Wang CM, Zhao YN, Li GD (2014) Eur J Inorg Chem 36:6239